Environmental Science: Atmospheres

ROYAL SOCIETY OF CHEMISTRY

PAPER

View Article Online
View Journal | View Issue

Open Access Article. Published on 26 September 2023. Downloaded on 11/8/2025 10:22:04 PM.
This article is licensed under a Creative Commons Attribution 3.0 Unported Licence.

Check for updates

Cite this: *Environ. Sci.: Atmos.*, 2023, **3**, 1642

Acoustic levitation with polarising optical microscopy (AL-POM): water uptake in a nanostructured atmospheric aerosol proxy†

Adam Milsom,[a] Adam M. Squires,[b] Christopher Brasnett,[cd] William N. Sharratt,[e] Annela M. Seddon[d] and Christian Pfrang *[af]

Received 9th June 2023
Accepted 8th September 2023

DOI: 10.1039/d3ea00083d

rsc.li/esatmospheres

Laboratory studies on levitated particles of atmospheric aerosol proxies have provided significant contributions to our understanding of aerosol processes. We present an experimental method combining acoustic levitation with polarising optical microscopy (AL-POM) to probe optically birefringent particles, such as the nanostructured surfactant atmospheric aerosol proxy studied here. Birefringent particles were subjected to a step increase in humidity. A decrease in birefringence was measured over time as a result of a nanostructure change, confirmed by complementary synchrotron X-ray scattering. A multi-layer water uptake model was created and fitted to the experimental data, revealing a water diffusion coefficient increase by *ca.* 5–6 orders of magnitude upon phase transition. This has implications for the timescale of water uptake in surfactant-containing aerosols and their atmospheric lifetimes. This experimental setup has strong potential to be used in conjunction with other levitation methods and in different contexts concerning birefringent materials such as crystallisation.

Environmental significance

The phase state of atmospheric aerosols is an important factor in determining the chemical lifetime of aerosol components, some of which affect cloud droplet formation and human health. This study presents a novel, non-invasive method of probing the phase state of levitated single aerosol particles undergoing humidity change. The application of a simplified model of particle water uptake allowed us to extract the water diffusion coefficient throughout humidifying particles of a cooking aerosol emission proxy – an important parameter in determining the timescales of water uptake and cloud droplet formation. There is potential to apply this technique to other atmospherically relevant systems to determine key physical parameters such as the diffusion coefficient of molecules in the condensed phase.

Introduction

Atmospheric aerosols facilitate cloud droplet formation[9] and have a significant impact on urban air quality.[10] The organic fraction of atmospheric aerosols can include a diverse range of molecules from alkanes to harmful polycyclic aromatic hydrocarbons (PAHs). This organic composition varies over time and between environments.[11,12]

Fatty acids are organic surfactants commonly observed in cooking and marine aerosol emissions.[13,14] Organic surfactant material affects cloud droplet nucleation by decreasing surface tension.[15] Oleic acid, a fatty acid surfactant and cooking emission marker,[11] has been shown to form a range of lyotropic liquid crystal (LLC) phases in contact with water.[16–18] The diffusion of small molecules through these phases is known to vary considerably due to the variable viscosities of these phases, compared with the free fatty acid.[19] Water uptake and diffusion through viscous particles has been an important topic of study due to the implications for cloud droplet nucleation.[1,4,20] We have previously shown that unsaturated fatty acid self-assembly can decrease reactivity with ozone by *ca.* an order of magnitude and that this could lengthen the atmospheric chemical lifetime by days.[21,22]

Surfactant molecule self-organisation and effects on water uptake in aerosols have much more general significance in different medical and commercial contexts. Inhaled therapeutic aerosols may deliver surfactants as active ingredients (as in the treatment of infant respiratory distress syndrome)[23,24] or

[a]*School of Geography, Earth and Environmental Sciences, University of Birmingham, Edgbaston, Birmingham, UK*
[b]*Department of Chemistry, University of Bath, South Building, Soldier Down Ln, Claverton Down, Bath, UK*
[c]*Groningen Biomolecular Sciences and Biotechnology Institute, University of Groningen, Groningen, The Netherlands*
[d]*HH Wills Physics Laboratory, School of Physics, University of Bristol, Bristol, UK*
[e]*School of Engineering, University of Liverpool, Liverpool, UK*
[f]*Department of Meteorology, University of Reading, Whiteknights, Earley Gate, Reading, UK*

† Electronic supplementary information (ESI) available. See DOI: https://doi.org/10.1039/d3ea00083d

© 2023 The Author(s). Published by the Royal Society of Chemistry

Open Access Article. Published on 26 September 2023. Downloaded on 11/8/2025 10:22:04 PM.
This article is licensed under a Creative Commons Attribution 3.0 Unported Licence.

excipients, where they effect hygroscopicity.[25] Hygroscopic growth and water uptake in inhaled drugs affects efficient delivery to the lungs.[26,27] Hygroscopicity and deliquescence of industrial surfactants in cleaning products causes caking, leading to processing problems.[28] Surfactants also effect efflorescence of salts within aerosols; in this way surfactant additives alter delivery of ionic active ingredients in agricultural sprays,[29] and lung surfactants in exhaled respiratory aerosols likely affect water uptake and salt efflorescence, which has been suggested as a mechanism for humidity-dependent viability of airborne pathogens.[30]

We present a new experimental approach to following water diffusion through LLC phases by coupling acoustic levitation with polarising optical microscopy (AL-POM). We followed the change from an optically birefringent (lamellar) to non-birefringent (close-packed inverse micellar) phase during humidification in a controlled gas-phase environment. A multi-layer water uptake model was created to reveal how water diffusivity changes during humidification, depending on the fatty acid molecular arrangement.

Methods

Preparation of the fatty acid aerosol proxy

Oleic acid (Sigma-Aldrich, 90% purity) and sodium oleate (Sigma-Aldrich, 99% purity) were dissolved as 10 wt% solutions in methanol, with gentle heating at ~50 °C until fully dissolved. Equal volumes of each solution were mixed to afford a 1 : 1 wt ratio solution of oleic acid and sodium oleate. This mixture was used throughout this study and is analogous to the mixture used for kinetic experiments on this proxy system.[21]

Acoustic levitation-polarising optical microscopy (AL-POM)

Acoustic levitation[2,5–8] of the fatty acid aerosol proxy was achieved by injecting ~20 μL of the proxy solution into the node of a modified commercial acoustic levitator (tec5, Oberursel, Germany) and allowing the solvent to evaporate, leaving behind the levitated sample. Multiple droplets can be levitated simultaneously. We assumed that the droplets were in thermal equilibrium with the surrounding atmosphere. This levitator has a fixed transducer frequency (100 kHz) and variable HF power (0.65–5 W). A concave reflector was positioned above the transducer and the transducer–reflector distance (typically 20–30 mm) was adjusted with a micrometre screw. The levitator was contained in a bespoke 3-D-printed chamber with ports to allow gas flow and viewing windows for optical and X-ray experiments (Fig. 1).

A cross-polarised optical system was established by attaching two light polarising filters on two opposing viewing windows of the levitation chamber. These filters were aligned in order to extinguish the light passing through both filters. An LED lamp was used as the light source. Only birefringent material placed between these filters would allow light to pass through, allowing detection of a birefringent levitated particle (see images in Fig. 1). A macroscope with a digital camera attached (Leica MC190 HD) was used to take images of the levitated particles

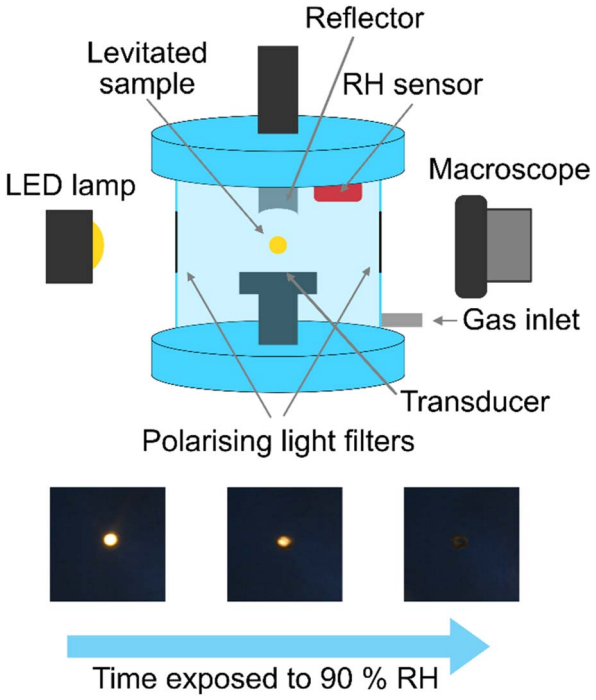

Fig. 1 Schematic representation of the AL-POM setup with typical images of a levitated sample during a humidity experiment, illustrating a reduction and then the disappearance of the particle birefringence.

from the side opposite to the incoming light. One image was taken every minute. A magnification of ×3.2 was used and the working distance was ~100 mm. Particle size was determined by measuring the diameter of the particle in pixels, a graticule was used to calibrate the particle size in physical units (μm). Particles were 165–260 μm in diameter. Particles tended to disintegrate into this diameter range after injection. The detailed image analysis procedure is described in the ESI.†

For higher resolution visualisation, droplets were imaged with a horizontal tube microscope comprising a long working distance infinity corrected objective (Mitutoyo 5X Plan Apo), tube lens (Mitutoyo MT-1) and CMOS camera (Basler ACA1920-155uc) yielding a resolution of 1.2 μm per pixel. A single-colour cold visible mounted green LED (530 nm Thorlabs M530L4) fitted with a collimation adapter (Thorlabs COP1-A) was used to illuminate the droplets. Cross-polarised imaging was achieved by mounting two dichroic film polarisers (Thorlabs LPVISE100-A); one mounted between the LED and the LED collimator and the other between the tube lens and the camera. The axes of the polarisers were oriented orthogonally to one another which, in the absence of a birefringent sample, yielded minimum light transmission.

Humidity was controlled using a bespoke Raspberry Pi (RPi) mini-computer system. This system controlled an air pump which pumped air through a glass humidifier. A humidity sensor (DHT22) was placed inside the levitation chamber and read by an Arduino mini-computer, which fed into the RPi humidity control software. For all experiments the starting relative humidity (RH) was ~50%. The levitation chamber was

Open Access Article. Published on 26 September 2023. Downloaded on 11/8/2025 10:22:04 PM.
This article is licensed under a Creative Commons Attribution 3.0 Unported Licence.

humidified to 90% RH for each experiment. The accuracy of the humidity sensor was 2–5% RH between 0–100% RH, as quoted by the manufacturer.

Acoustic levitation small-angle X-ray scattering (SAXS)

Small-angle X-ray scattering (SAXS) probes samples on the nanoscale to reveal how molecules aggregate together.[31] The nanostructured sample is illuminated by X-rays, some of which are scattered. Plots of scattered intensity *vs.* q (momentum transfer – related to scattering angle) allow for determination of which (if any) arrangement is present in a sample by identifying Bragg scattering peak positions.[32]

SAXS measurements were carried out on levitated particles on the I22 beamline at the Diamond Light Source synchrotron X-ray facility.[33] Levitated particles were exposed to X-rays of 12.4 keV energy in 1 s frames using a Pilatus P3-2M detector. The size of the X-ray beam used was ~22 μm × 19 μm. We assume that any droplet temperature rise associated with X-ray irradiation is negligible due to the small beam in comparison to the droplet and the short exposure time.

Multi-layer water uptake model

We have devised a multi-layer approach to spatially and temporally resolve the uptake and diffusion of water through a self-assembled particle, incorporating changes in diffusivity caused by water content-dependent phase changes. This modelling approach is similar to those which resolve aerosol and surface and bulk chemistry[34–38] and ones which consider water uptake into viscous particles.[4,20,39] The multi-layer model is described in detail in the ESI†.

Water diffusion was treated as composition-dependent and is related to the mole fraction of lamellar phase in layer I ($f_{\mathrm{lam},i}$) by a Vignes-type relationship:[40]

$$D_{\mathrm{w},i} = (D_{\mathrm{w,lam}})^{f_{\mathrm{lam},i}} \times (D_{\mathrm{w,mic}})^{(1-f_{\mathrm{lam},i})}$$

Where $D_{\mathrm{b,w,lam}}$ and $D_{\mathrm{b,w,mic}}$ are the diffusivities of water in the lamellar phase and close-packed inverse micellar phase, respectively.

We could not directly determine $D_{\mathrm{w}}^{\mathrm{o}}$ in these phases with this experiment, though there have been NMR-based diffusion measurements on similar systems.[41] We use this literature value of $D_{\mathrm{w}}^{\mathrm{o}}$ in order to place the model results in a physically meaningful context (see later).

The model parameters were optimised using a differential evolution algorithm available in the SciPy package in Python.[42,43] The initial population of parameter sets were sampled using a latin hypercube, which ensures the initial population evenly covers the available parameter space. The resulting population was evolved in parallel over 20 cpu cores. This approach to global optimisation is similar to that of Berkemeier *et al.*, who used an initial Monte Carlo sampling method.[44] The number of model layers was adjusted to maintain the same spatial resolution for each particle (*i.e.* 200 layers for the 220 μm diameter particle; 236 layers for the 260 μm particle).

Results and discussion

Identification of surfactant arrangements at low and high humidity

In order to confirm which molecular arrangements were present at room (~50% RH) and high (~90% RH) humidity, samples were levitated and SAXS patterns were taken at a synchrotron X-ray source.[33] Fig. 2a shows the 2-D scattering pattern from the top edge of a levitated particle ~3 min after levitation at room humidity. This scattering pattern corresponds to the lamellar phase. This lamellar phase is highly oriented due to the lack of a diffuse scattering ring for each lamellar Bragg peak (see ESI† for a scattering pattern from a randomly oriented lamellar phase showing diffuse scattering rings). This kind of surface orientation has been observed previously in levitated droplets of LLC phases[3] and in nanometre-scale films of this system.[45]

Diffusion is highly anisotropic in the lamellar phase.[46,47] If lamellar bilayers are highly aligned parallel to the droplet surface (as observed here), water uptake is likely to be affected. This justifies the explicit separation of water uptake into the lamellar and inverse micellar phase in the surface layer of the model (see ESI†).

At high humidity, we observed the ordered inverse micellar phase with *Fd*3*m* symmetry after ~10 min (Fig. 2b). The close-

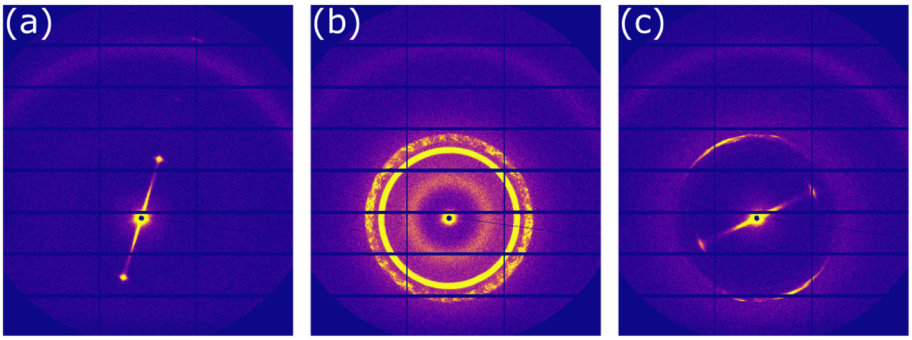

Fig. 2 2-D SAXS patterns from a levitated oleic acid–sodium oleate particle. (a) The edge of the particle at the beginning of the experiment (low RH), showing a highly oriented lamellar phase. (b) The centre of the same particle at high humidity (90% RH), showing the *Fd*3*m* close-packed inverse micellar phase. (c) The edge of the same particle at 90% RH showing some orientation of the *Fd*3*m* phase.

 © 2023 The Author(s). Published by the Royal Society of Chemistry

Open Access Article. Published on 26 September 2023. Downloaded on 11/8/2025 10:22:04 PM. This article is licensed under a Creative Commons Attribution 3.0 Unported Licence.

packed inverse micelles present in this phase have varying sizes and restricted water mobility.[41,48]

The close-packed inverse micellar phase is isotropic and is not observable by POM. This is in agreement with the levitation-POM humidity experiment where an optically anisotropic (lamellar) phase is transformed into an optically isotropic phase (close-packed inverse micellar) (compare typical images in Fig. 1).

Following water uptake during humidification

We levitated two particles of 220 and 260 μm diameter simultaneously and followed their respective water uptakes with the levitation-POM experiment. A single set of optimised model parameters fit reasonably well with these data (Fig. 3a). A separate model optimisation using the data from a 190 μm particle returned optimised parameters which were similar to those obtained by the simultaneous particle optimisation (Fig. 3b and c). This set of parameters fit well to both the 190 and 165 μm particles, which were levitated in separate experiments. Optimised model parameters are presented in the ESI.†

The water uptake model did not account for any intermediate phases that could have formed when transitioning from the anhydrous lamellar to the close-packed inverse micellar phase. It is possible that a disordered (rather than close-packed) inverse micellar phase forms as an intermediate phase.[49] This has been observed in experiments on a crystalline form of this proxy.[50] The less viscous nature of the disordered inverse micellar phase, which is also non-birefringent, could account for some of the difference between the model fits and experimental data.

The diffusion coefficient of water in the oleic acid-sodium oleate close-packed inverse micellar phase has been experimentally determined to be 2.4×10^{-8} cm^2 s^{-1}.[41] We used this to convert model diffusion coefficients to physically meaningful values. The water diffusion coefficient in the lamellar phase was determined from the model fit as 7.0×10^{-14} cm^2 s^{-1}. This puts water diffusivity in these observed phases in the semi-solid regime.[51] This value was obtained from the set of model parameters fitting to the 220 and 260 μm diameter particles (Fig. 3a), which were levitated simultaneously and had the most experimental measurements to fit to.

Water diffusion through the anhydrous lamellar phase is *ca.* 5–6 orders of magnitude slower than in the close-packed inverse micellar phase, demonstrating the sensitivity of water diffusion to particle nanostructure and viscosity. Note that the lamellar phase studied here is anhydrous and not a lyotropic system (*i.e.* it is without a solvent). Without water acting as a plasticiser, anhydrous lamellar bilayers are more restricted in their movement, increasing their rigidity and viscosity.[52] The spacing between fatty acid chains in this lamellar phase has been measured to be 0.441 nm.[21] This is within double the molecular diameter of water (*ca.* 0.27 nm).[53] The steric restriction imposed by the spacing between fatty acid alkyl chains helps explain why water diffusion through the anhydrous lamellar phase is so much slower than in the close-packed inverse micellar phase.

A steep water diffusion gradient is established within the particle during humidification (Fig. 4a). As more water is taken up, the lamellar phase transitions to the close-packed inverse micellar phase, affecting D_w *via* the Vignes-type relationship described earlier.

Particle water activity (a_w) and lamellar phase mole fraction (f_{lam}) follow a similar trend, highlighting the link between water content, phase transition and water diffusivity (Fig. 4b and c). Acoustic levitation does not allow us to directly determine the mass or volume of water in this case. Time-resolved size information is sacrificed in AL-POM due to the loss of particle brightness during humidity induced phase transitions. This is because we used the brightness of a particle as a way of identifying the particle and determining particle diameter against the dark background.

Data collected by AL-POM could be used to follow chemical reactions which destroy the birefringent phases being probed. Depth-resolved model outputs such as those presented in Fig. 4 are possible with kinetic multi-layer models, which have become the state-of-the-art in aerosol science.[34,36–38,54] AL-POM only probes birefringent phases, therefore it is specific and could be used for chemical kinetics in a similar way to the use of SAXS as a tool to measure reaction kinetics of specific self-

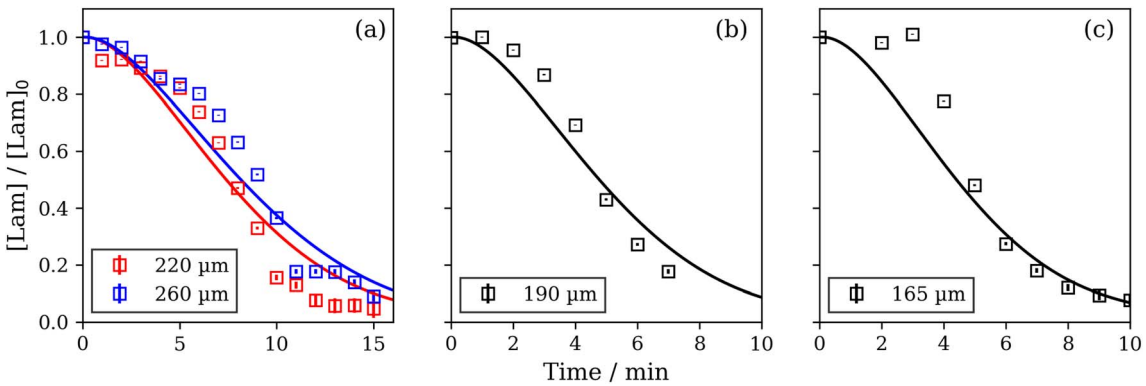

Fig. 3 Plots of the normalised amount of lamellar phase ([Lam]/[Lam]$_0$) *vs.* time with corresponding model fits (solid lines) for each particle diameter. (a) An experiment where two particles were levitated simultaneously. (b) and (c) Two particles levitated separately – the optimised model fits for these two experiments returned slightly different parameters to the ones optimised in panel (a).

Open Access Article. Published on 26 September 2023. Downloaded on 11/8/2025 10:22:04 PM.
This article is licensed under a Creative Commons Attribution 3.0 Unported Licence.

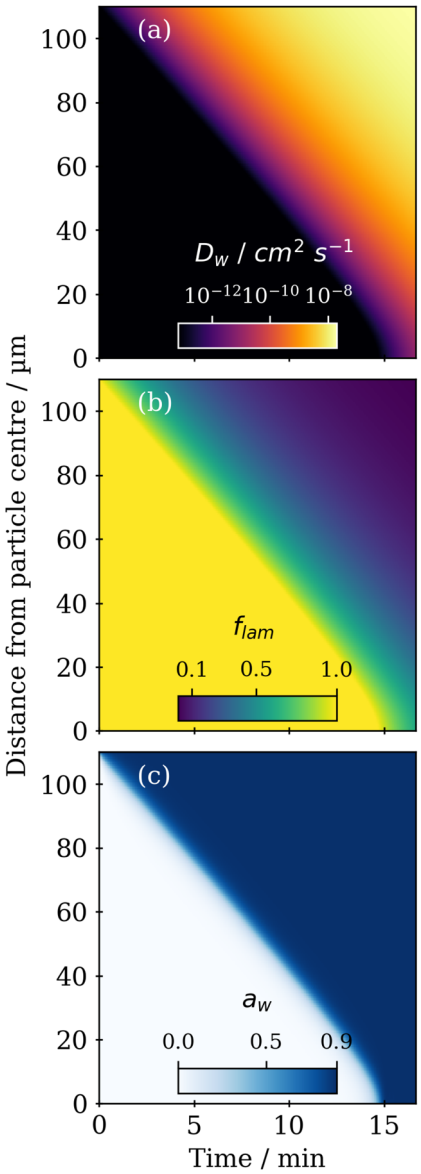

Fig. 4 Model outputs for a 110 µm radius particle exposed to 90% RH. (a) Evolution of the water diffusion coefficient (D_w) throughout the humidifying particle. (b) Evolution of the mole fraction of lamellar phase (f_{lam}) throughout the particle. (c) Evolution of water activity (a_w) throughout the particle.

organised structures.[21] Application of a kinetic multi-layer model to those kinetic data could then provide insights into the real-world impact of a particular phenomenon (*e.g.* how surfactant self-organisation impacts the chemical lifetime of atmospheric aerosol constituents).[22]

Atmospheric implications

The D_w range derived from our model ($\sim 10^{-14}$–10^{-8} cm^2 s^{-1}) is similar to measurements of D_w in water-sucrose mixtures ($\sim 10^{-13}$–10^{-6} cm^2 s^{-1}), placing this nanostructured proxy system in a similar water diffusion regime.

There is a strong dependence of D_w on molecular arrangement, with D_w increasing by *ca.* 5–6 orders of magnitude upon the lamellar-to-ordered inverse micellar phase transition. We thus have direct evidence that water diffusion is affected by molecular arrangement, similar to the effect that nanostructure formation has on the oxidation reactivity of the same proxy system.[21]

The link between aerosol phase state and atmospheric lifetime is well-established and has implications for the long-range transport of aerosols and their impact on the climate and pollution.[55–57] We have shown here that the diffusivity of water though a nanostructured surfactant aerosol proxy is impacted by the arrangement of these surfactant molecules, which itself is determined by the amount of water in the system.

With AL-POM, it is also possible to determine whether humidity-induced phase transitions are between amorphous or crystalline phases, which are often optically birefringent if the crystal structure is anisotropic. This is of importance when considering the interaction of aerosol particles with water vapour.[58]

The AL-POM experimental setup is possible in a standard chemistry laboratory and could be coupled with other forms of levitation such as an electro-dynamic balance (EDB). Coupled with the improved optics, optical textures can be distinguished in a levitated birefringent particle with the increased resolution. We demonstrated this by watching a non-birefringent methanolic solution of oleic acid–sodium oleate–fructose (1 : 1 : 1 wt) evaporate to form a birefringent phase (Fig. 5). There is therefore the possibility to identify phase separation between birefringent and non-birefringent domains within levitated droplets. Phase separation is of particular interest in the

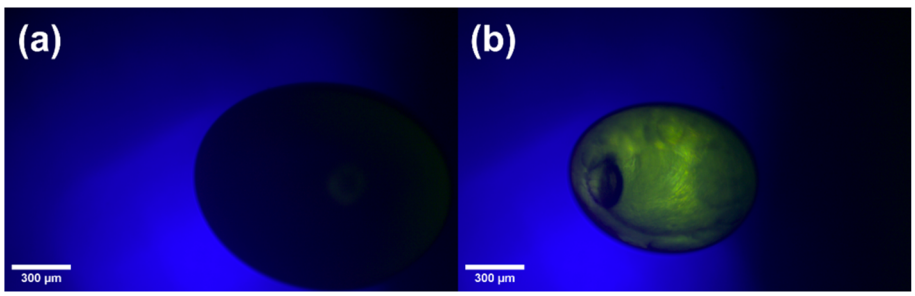

Fig. 5 Cross-polarised images of acoustically levitated droplets of oleic acid–sodium oleate–fructose (1 : 1 : 1 wt) evaporating from a 10 wt% methanolic solution. (a) The start of the experiment where the initial droplet is a solution of oleic acid-sodium oleate-fructose in methanol. (b) The end of the experiment where methanol has mostly evaporated from the droplet to leave a birefringent phase.

 © 2023 The Author(s). Published by the Royal Society of Chemistry

Open Access Article. Published on 26 September 2023. Downloaded on 11/8/2025 10:22:04 PM.
This article is licensed under a Creative Commons Attribution 3.0 Unported Licence.

atmospheric aerosol community, with implications for cloud droplet nucleation.[59–61] Even if no high-quality camera is available, the phase transition observed during this study is still observable with a standard computer webcam (as demonstrated in the ESI section S5†).

Conclusions

This work has shown that a comparably facile laboratory-based setup (AL-POM) consisting of polarising filters, an acoustic levitator, a camera and a light source can return physically meaningful results provided the sample environment can be controlled. LLC phase transitions have previously been followed in acoustically levitated droplets when coupled with X-ray scattering techniques, providing a more detailed insight into the nanostructure of the particle.[3,16,50] However, this requires rather specialist instrumentation and access to a synchrotron light source.

The simple composition-dependent parameterisation of water diffusivity, along with the inclusion and parameterisation of phase transition boundaries in the model, means that the model could be applied to more complex systems such as the inverse micellar (non-birefringent)-hydrated lamellar (birefringent)-inverse cubic (non-birefringent) phase transitions observed for the phytantriol-glycerol system.[62] With prior knowledge of the diffusion coefficient of water through at least one of these phases, predictions could be made regarding the diffusivity of water through such phases. AL-POM could be applicable to studies concerning atmospheric and respiratory aerosol, drug delivery, and cosmetics.

Conflicts of interest

There are no conflicts to declare.

Acknowledgements

AM acknowledges funding by the NERC SCENARIO DTP (NE/L002566/1) and support from the NERC CENTA DTP. This work was carried out with the support of the Diamond Light Source (UK), instrument I22 (proposals SM23852 and SM17791). Nick Terrill, Andy Smith, Tim Snow and Olga Shebanova (DLS) are acknowledged for their support during experiments at the DLS. The computations described in this paper were performed using the University of Birmingham's BlueBEAR HPC service, which provides a High Performance Computing service to the University's research community. This research has also been supported by the Natural Environment Research Council (grant no. NE/T00732X/1, NE/G000883/1 and NE/G019231/1) and the Royal Society (grant no. 2007/R2).

References

1 J. F. Davies and K. R. Wilson, Raman Spectroscopy of Isotopic Water Diffusion in Ultraviscous, Glassy, and Gel States in Aerosol by Use of Optical Tweezers, *Anal. Chem.*, 2016, **88**, 2361–2366.

2 M. S. Westphall, K. Jorabchi and L. M. Smith, Mass spectrometry of acoustically levitated droplets, *Anal. Chem.*, 2008, **80**, 5847–5853.

3 A. M. Seddon, S. J. Richardson, K. Rastogi, T. S. Plivelic, A. M. Squires and C. Pfrang, Control of Nanomaterial Self-Assembly in Ultrasonically Levitated Droplets, *J. Phys. Chem. Lett.*, 2016, **7**, 1341–1345.

4 B. Zobrist, V. Soonsin, B. P. Luo, U. K. Krieger, C. Marcolli, T. Peter and T. Koop, Ultra-slow water diffusion in aqueous sucrose glasses, *Phys. Chem. Chem. Phys.*, 2011, **13**, 3514–3526.

5 N. J. Mason, E. A. Drage, S. M. Webb, A. Dawes, R. McPheat and G. Hayes, The spectroscopy and chemical dynamics of microparticles explored using an ultrasonic trap, *Faraday Discuss.*, 2007, **137**, 367–376.

6 L. Cohen, M. I. Quant, M. I. Quant, D. J. Donaldson and D. J. Donaldson, Real-Time Measurements of pH Changes in Single, Acoustically Levitated Droplets Due to Atmospheric Multiphase Chemistry, *ACS Earth Space Chem.*, 2020, **4**, 854–861.

7 U. K. Krieger, C. Marcolli and J. P. Reid, Exploring the complexity of aerosol particle properties and processes using single particle techniques, *Chem. Soc. Rev.*, 2012, **41**, 6631–6662.

8 S. Santesson and S. Nilsson, Airborne chemistry: Acoustic levitation in chemical analysis, *Anal. Bioanal. Chem.*, 2004, **378**, 1704–1709.

9 O. Boucher, D. Randall, P. Artaxo, C. Bretherton, G. Feingold, P. Forster, V.-M. Kerminen, Y. Kondo, H. Liao, U. Lohmann, P. Rasch, S. K. Satheesh, S. Sherwood, B. Stevens and X. Y. Zhang, in *Climate Change 2013 - The Physical Science Basis*, ed. Intergovernmental Panel on Climate Change, Cambridge University Press, Cambridge, 2013, pp. 571–658.

10 M. Kulmala, L. Dada, K. R. Daellenbach, C. Yan, D. Stolzenburg, J. Kontkanen, E. Ezhova, S. Hakala, S. Tuovinen, T. V. Kokkonen, M. Kurppa, R. Cai, Y. Zhou, R. Yin, R. Baalbaki, T. Chan, B. Chu, C. Deng, Y. Fu, M. Ge, H. He, L. Heikkinen, H. Junninen, Y. Liu, Y. Lu, W. Nie, A. Rusanen, V. Vakkari, Y. Wang, G. Yang, L. Yao, J. Zheng, J. Kujansuu, J. Kangasluoma, T. Petäjä, P. Paasonen, L. Järvi, D. Worsnop, A. Ding, Y. Liu, L. Wang, J. Jiang, F. Bianchi and V.-M. Kerminen, Is reducing new particle formation a plausible solution to mitigate particulate air pollution in Beijing and other Chinese megacities?, *Faraday Discuss.*, 2021, **226**, 334–347.

11 Q. Wang, X. He, M. Zhou, D. D. Huang, L. Qiao, S. Zhu, Y. G. Ma, H. L. Wang, L. Li, C. Huang, X. H. H. Huang, W. Xu, D. Worsnop, A. H. Goldstein, H. Guo, J. Z. Yu, C. Huang and J. Z. Yu, Hourly Measurements of Organic Molecular Markers in Urban Shanghai, China: Primary Organic Aerosol Source Identification and Observation of Cooking Aerosol Aging, *ACS Earth Space Chem.*, 2020, **4**, 1670–1685.

12 J. L. Jimenez, M. R. Canagaratna, N. M. Donahue, A. S. H. Prevot, Q. Zhang, J. H. Kroll, P. F. DeCarlo, J. D. Allan, H. Coe, N. L. Ng, A. C. Aiken, K. S. Docherty, I. M. Ulbrich, A. P. Grieshop, A. L. Robinson, J. Duplissy,

Open Access Article. Published on 26 September 2023. Downloaded on 11/8/2025 10:22:04 PM.
This article is licensed under a Creative Commons Attribution 3.0 Unported Licence.

J. D. Smith, K. R. Wilson, V. A. Lanz, C. Hueglin, Y. L. Sun, J. Tian, A. Laaksonen, T. Raatikainen, J. Rautiainen, P. Vaattovaara, M. Ehn, M. Kulmala, J. M. Tomlinson, D. R. Collins, M. J. Cubison, J. Dunlea, J. A. Huffman, T. B. Onasch, M. R. Alfarra, P. I. Williams, K. Bower, Y. Kondo, J. Schneider, F. Drewnick, S. Borrmann, S. Weimer, K. Demerjian, D. Salcedo, L. Cottrell, R. Griffin, A. Takami, T. Miyoshi, S. Hatakeyama, A. Shimono, J. Y. Sun, Y. M. Zhang, K. Dzepina, J. R. Kimmel, D. Sueper, J. T. Jayne, S. C. Herndon, A. M. Trimborn, L. R. Williams, E. C. Wood, A. M. Middlebrook, C. E. Kolb, U. Baltensperger and D. R. Worsnop, Evolution of Organic Aerosols in the Atmosphere, *Science*, 2009, **326**, 1525–1529.

13 C. A. Alves, E. D. Vicente, M. Evtyugina, A. M. Vicente, T. Nunes, F. Lucarelli, G. Calzolai, S. Nava, A. I. Calvo, C. del B. Alegre, F. Oduber, A. Castro and R. Fraile, Indoor and outdoor air quality: A university cafeteria as a case study, *Atmos. Pollut. Res.*, 2020, **11**, 531–544.

14 H. Tervahattu, J. Juhanoja, V. Vaida, A. F. Tuck, J. V. Niemi, K. Kupiainen, M. Kulmala and H. Vehkamäki, Fatty acids on continental sulfate aerosol particles, *J. Geophys. Res. D: Atmos.*, 2005, **110**, 1–9.

15 J. Ovadnevaite, A. Zuend, A. Laaksonen, K. J. Sanchez, G. Roberts, D. Ceburnis, S. Decesari, M. Rinaldi, N. Hodas, M. C. Facchini, J. H. Seinfeld and C. O'Dowd, Surface tension prevails over solute effect in organic-influenced cloud droplet activation, *Nature*, 2017, **546**, 637–641.

16 C. Pfrang, K. Rastogi, E. R. Cabrera-Martinez, A. M. Seddon, C. Dicko, A. Labrador, T. S. Plivelic, N. Cowieson and A. M. Squires, Complex three-dimensional self-assembly in proxies for atmospheric aerosols, *Nat. Commun.*, 2017, **8**, 1724.

17 S. Mele, O. Söderman, H. Ljusberg-Wahrén, K. Thuresson, M. Monduzzi and T. Nylander, Phase behavior in the biologically important oleic acid/sodium oleate/water system, *Chem. Phys. Lipids*, 2018, **211**, 30–36.

18 A. Milsom, A. M. Squires, I. Quant, N. J. Terrill, S. Huband, B. Woden, E. R. Cabrera-Martinez and C. Pfrang, Exploring the Nanostructures Accessible to an Organic Surfactant Atmospheric Aerosol Proxy, *J. Phys. Chem. A*, 2022, **126**, 7331–7341.

19 A. Zabara and R. Mezzenga, Controlling molecular transport and sustained drug release in lipid-based liquid crystalline mesophases, *J. Controlled Release*, 2014, **188**, 31–43.

20 H. C. Price, J. Mattsson, Y. Zhang, A. K. Bertram, J. F. Davies, J. W. Grayson, S. T. Martin, D. O'Sullivan, J. P. Reid, A. M. J. Rickards and B. J. Murray, Water diffusion in atmospherically relevant α-pinene secondary organic material, *Chem. Sci.*, 2015, **6**, 4876–4883.

21 A. Milsom, A. M. Squires, B. Woden, N. J. Terrill, A. D. Ward and C. Pfrang, The persistence of a proxy for cooking emissions in megacities: a kinetic study of the ozonolysis of self-assembled films by simultaneous small and wide angle X-ray scattering (SAXS/WAXS) and Raman microscopy, *Faraday Discuss.*, 2021, **226**, 364–381.

22 A. Milsom, A. M. Squires, A. D. Ward and C. Pfrang, The impact of molecular self-organisation on the atmospheric fate of a cooking aerosol proxy, *Atmos. Chem. Phys.*, 2022, **22**, 4895–4907.

23 G. Pohlmann, P. Iwatschenko, W. Koch, H. Windt, M. Rast, M. G. de Abreu, F. J. H. Taut and C. De Muynck, A Novel Continuous Powder Aerosolizer (CPA) for Inhalative Administration of Highly Concentrated Recombinant Surfactant Protein-C (rSP-C) Surfactant to Preterm Neonates, *J. Aerosol Med. Pulm. Drug Delivery*, 2013, **26**, 370–379.

24 S. Boc, M. A. M. Momin, D. R. Farkas, W. Longest and M. Hindle, Development and Characterization of Excipient Enhanced Growth (EEG) Surfactant Powder Formulations for Treating Neonatal Respiratory Distress Syndrome, *AAPS PharmSciTech*, 2021, **22**, 1–12.

25 Y. Cui, X. Zhang, W. Wang, Z. Huang, Z. Zhao, G. Wang, S. Cai, H. Jing, Y. Huang, X. Pan and C. Wu, Moisture-Resistant Co-Spray-Dried Netilmicin with l-Leucine as Dry Powder Inhalation for the Treatment of Respiratory Infections, *Pharmaceutics*, 2018, **10**, 252.

26 P. Worth Longest and M. Hindle, Numerical Model to Characterize the Size Increase of Combination Drug and Hygroscopic Excipient Nanoparticle Aerosols, *Aerosol Sci. Technol.*, 2011, **45**, 884–899.

27 A. J. Hickey and T. B. Martonen, Behavior of Hygroscopic Pharmaceutical Aerosols and the Influence of Hydrophobic Additives, *Pharm. Res.*, 1993, **10**, 1–7.

28 U. Zafar, V. Vivacqua, G. Calvert, M. Ghadiri and J. A. S. Cleaver, A review of bulk powder caking, *Powder Technol.*, 2017, **313**, 389–401.

29 E. C. Tredenick, T. W. Farrell and W. A. Forster, Mathematical Modelling of Hydrophilic Ionic Fertiliser Diffusion in Plant Cuticles: Lipophilic Surfactant Effects, *Plants*, 2019, **8**, 202.

30 H. P. Oswin, A. E. Haddrell, M. Otero-Fernandez, J. F. S. Mann, T. A. Cogan, T. G. Hilditch, J. Tian, D. A. Hardy, D. J. Hill, A. Finn, A. D. Davidson and J. P. Reid, The dynamics of SARS-CoV-2 infectivity with changes in aerosol microenvironment, *Proc. Natl. Acad. Sci.*, 2022, **119**, 1–11.

31 T. Li, A. J. Senesi and B. Lee, Small Angle X-ray Scattering for Nanoparticle Research, *Chem. Rev.*, 2016, **116**, 11128–11180.

32 C. V. Kulkarni, W. Wachter, G. Iglesias-Salto, S. Engelskirchen and S. Ahualli, Monoolein: a magic lipid?, *Phys. Chem. Chem. Phys.*, 2011, **13**, 3004–3021.

33 A. J. Smith, S. G. Alcock, L. S. Davidson, J. H. Emmins, J. C. Hiller Bardsley, P. Holloway, M. Malfois, A. R. Marshall, C. L. Pizzey, S. E. Rogers, O. Shebanova, T. Snow, J. P. Sutter, E. P. Williams and N. J. Terrill, I22: SAXS/WAXS beamline at Diamond Light Source - an overview of 10 years operation, *J. Synchrotron Radiat.*, 2021, **28**, 939–947.

34 M. Shiraiwa, C. Pfrang and U. Pöschl, Kinetic multi-layer model of aerosol surface and bulk chemistry (KM-SUB): The influence of interfacial transport and bulk diffusion on the oxidation of oleic acid by ozone, *Atmos. Chem. Phys.*, 2010, **10**, 3673–3691.

 © 2023 The Author(s). Published by the Royal Society of Chemistry

Open Access Article. Published on 26 September 2023. Downloaded on 11/8/2025 10:22:04 PM.
This article is licensed under a Creative Commons Attribution 3.0 Unported Licence.

35 U. Pöschl, Y. Rudich and M. Ammann, Kinetic model framework for aerosol and cloud surface chemistry and gas-particle interactions - Part 1: General equations, parameters, and terminology, *Atmos. Chem. Phys.*, 2007, **7**, 5989–6023.

36 A. Milsom, A. Lees, A. M. Squires and C. Pfrang, MultilayerPy (v1.0): a Python-based framework for building, running and optimising kinetic multi-layer models of aerosols and films, *Geosci. Model Dev.*, 2022, **15**, 7139–7151.

37 M. Shiraiwa, C. Pfrang, T. Koop and U. Pöschl, Kinetic multi-layer model of gas-particle interactions in aerosols and clouds (KM-GAP): Linking condensation, evaporation and chemical reactions of organics, oxidants and water, *Atmos. Chem. Phys.*, 2012, **12**, 2777–2794.

38 T. Berkemeier, A. Mishra, C. Mattei, A. J. Huisman, U. K. Krieger and U. Pöschl, Ozonolysis of Oleic Acid Aerosol Revisited: Multiphase Chemical Kinetics and Reaction Mechanisms, *ACS Earth Space Chem.*, 2021, **5**, 3313–3323.

39 D. M. Lienhard, A. J. Huisman, D. L. Bones, Y. F. Te, B. P. Luo, U. K. Krieger and J. P. Reid, Retrieving the translational diffusion coefficient of water from experiments on single levitated aerosol droplets, *Phys. Chem. Chem. Phys.*, 2014, **16**, 16677–16683.

40 A. Vignes, Variation in Diffusion Coefficient with Composition, *Ind. Eng. Chem. Fundam.*, 1966, **5**, 189–199.

41 Y. Hendrikx, P. Sotta, J. M. Seddon, Y. Dutheillet and E. A. Bartle, NMR self-diffusion measurements in inverse micellar cubic phases, *Liq. Cryst.*, 1994, **16**, 893–903.

42 P. Virtanen, R. Gommers, T. E. Oliphant, M. Haberland, T. Reddy, D. Cournapeau, E. Burovski, P. Peterson, W. Weckesser, J. Bright, S. J. van der Walt, M. Brett, J. Wilson, K. J. Millman, N. Mayorov, A. R. J. Nelson, E. Jones, R. Kern, E. Larson, C. J. Carey, İ. Polat, Y. Feng, E. W. Moore, J. VanderPlas, D. Laxalde, J. Perktold, R. Cimrman, I. Henriksen, E. A. Quintero, C. R. Harris, A. M. Archibald, A. H. Ribeiro, F. Pedregosa, P. van Mulbregt, A. Vijaykumar, A. Pietro Bardelli, A. Rothberg, A. Hilboll, A. Kloeckner, A. Scopatz, A. Lee, A. Rokem, C. N. Woods, C. Fulton, C. Masson, C. Häggström, C. Fitzgerald, D. A. Nicholson, D. R. Hagen, D. V. Pasechnik, E. Olivetti, E. Martin, E. Wieser, F. Silva, F. Lenders, F. Wilhelm, G. Young, G. A. Price, G. L. Ingold, G. E. Allen, G. R. Lee, H. Audren, I. Probst, J. P. Dietrich, J. Silterra, J. T. Webber, J. Slavič, J. Nothman, J. Buchner, J. Kulick, J. L. Schönberger, J. V. de Miranda Cardoso, J. Reimer, J. Harrington, J. L. C. Rodríguez, J. Nunez-Iglesias, J. Kuczynski, K. Tritz, M. Thoma, M. Newville, M. Kümmerer, M. Bolingbroke, M. Tartre, M. Pak, N. J. Smith, N. Nowaczyk, N. Shebanov, O. Pavlyk, P. A. Brodtkorb, P. Lee, R. T. McGibbon, R. Feldbauer, S. Lewis, S. Tygier, S. Sievert, S. Vigna, S. Peterson, S. More, T. Pudlik, T. Oshima, T. J. Pingel, T. P. Robitaille, T. Spura, T. R. Jones, T. Cera, T. Leslie, T. Zito, T. Krauss, U. Upadhyay, Y. O. Halchenko and Y. Vázquez-Baeza, SciPy 1.0: fundamental algorithms for scientific computing in Python, *Nat. Methods*, 2020, **17**, 261–272.

43 R. Storn and K. Price, Differential Evolution – A Simple and Efficient Heuristic for global Optimization over Continuous Spaces, *J. Glob. Optim.*, 1997, **11**, 341–359.

44 T. Berkemeier, M. Ammann, U. K. Krieger, T. Peter, P. Spichtinger, U. Pöschl, M. Shiraiwa and A. J. Huisman, Technical note: Monte Carlo genetic algorithm (MCGA) for model analysis of multiphase chemical kinetics to determine transport and reaction rate coefficients using multiple experimental data sets, *Atmos. Chem. Phys.*, 2017, **17**, 8021–8029.

45 A. Milsom, A. M. Squires, M. W. A. Skoda, P. Gutfreund, E. Mason, N. J. Terrill and C. Pfrang, The evolution of surface structure during simulated atmospheric ageing of nano-scale coatings of an organic surfactant aerosol proxy, *Environ. Sci.: Atmos.*, 2022, **2**, 964–977.

46 G. Lindblom and H. Wennerström, Amphiphile diffusion in model membrane systems studied by pulsed NMR, *Biophys. Chem.*, 1977, **6**, 167–171.

47 G. Lindblom and G. Orädd, NMR Studies of translational diffusion in lyotropic liquid crystals and lipid membranes, *Prog. Nucl. Magn. Reson. Spectrosc.*, 1994, **26**, 483–515.

48 M. Pouzot, R. Mezzenga, M. Leser, L. Sagalowicz, S. Guillote and O. Glatter, Structural and rheological investigation of Fd3m inverse micellar cubic phases, *Langmuir*, 2007, **23**, 9618–9628.

49 J. M. Seddon, E. A. Bartle and J. Mingins, Inverse cubic liquid-crystalline phases of phospholipids and related lyotropic systems, *J. Phys.: Condens.Matter*, 1990, **2**, SA285–SA290.

50 A. Milsom, A. M. Squires, J. A. Boswell, N. J. Terrill, A. D. Ward and C. Pfrang, An organic crystalline state in ageing atmospheric aerosol proxies: Spatially resolved structural changes in levitated fatty acid particles, *Atmos. Chem. Phys.*, 2021, **21**, 15003–15021.

51 M. Shiraiwa, M. Ammann, T. Koop and U. Poschl, Gas uptake and chemical aging of semisolid organic aerosol particles, *Proc. Natl. Acad. Sci. U. S. A.*, 2011, **108**, 11003–11008.

52 M. Youssry, L. Coppola, I. Nicotera and C. Morán, Swollen and collapsed lyotropic lamellar rheology, *J. Colloid Interface Sci.*, 2008, **321**, 459–467.

53 P. Schatzberg, Molecular diameter of water from solubility and diffusion measurements, *J. Phys. Chem.*, 1967, **71**, 4569–4570.

54 T. Berkemeier, M. Krüger, A. Feinberg, M. Müller, U. Pöschl and U. K. Krieger, Accelerating models for multiphase chemical kinetics through machine learning with polynomial chaos expansion and neural networks, *Geosci. Model Dev.*, 2023, **16**, 2037–2054.

55 S. Zhou, B. C. H. Hwang, P. S. J. Lakey, A. Zuend, J. P. D. Abbatt and M. Shiraiwa, Multiphase reactivity of polycyclic aromatic hydrocarbons is driven by phase separation and diffusion limitations, *Proc. Natl. Acad. Sci. U. S. A.*, 2019, **116**, 11658–11663.

56 Q. Mu, M. Shiraiwa, M. Octaviani, N. Ma, A. Ding, H. Su, G. Lammel, U. Pöschl and Y. Cheng, Temperature effect on phase state and reactivity controls atmospheric multiphase

Open Access Article. Published on 26 September 2023. Downloaded on 11/8/2025 10:22:04 PM.
This article is licensed under a Creative Commons Attribution 3.0 Unported Licence.

chemistry and transport of PAHs, *Sci. Adv.*, 2018, **4**, eaap7314.

57 J. H. Slade, M. Shiraiwa, A. Arangio, H. Su, U. Pöschl, J. Wang and D. A. Knopf, Cloud droplet activation through oxidation of organic aerosol influenced by temperature and particle phase state, *Geophys. Res. Lett.*, 2017, **44**, 1583–1591.

58 E. Mikhailov, S. Vlasenko, S. T. Martin, T. Koop and U. Pöschl, Amorphous and crystalline aerosol particles interacting with water vapor: Conceptual framework and experimental evidence for restructuring, phase transitions and kinetic limitations, *Atmos. Chem. Phys.*, 2009, **9**, 9491–9522.

59 M. A. Freedman, Liquid–Liquid Phase Separation in Supermicrometer and Submicrometer Aerosol Particles, *Acc. Chem. Res.*, 2020, **53**, 1102–1110.

60 Y. Huang, F. Mahrt, S. Xu, M. Shiraiwa, A. Zuend and A. K. Bertram, Coexistence of three liquid phases in individual atmospheric aerosol particles, *Proc. Natl. Acad. Sci.*, 2021, **118**(16), e2102512118.

61 F. Mahrt, L. Peng, J. Zaks, Y. Huang, P. E. Ohno, N. R. Smith, F. K. A. Gregson, Y. Qin, C. L. Faiola, S. T. Martin, S. A. Nizkorodov, M. Ammann and A. K. Bertram, Not all types of secondary organic aerosol mix: two phases observed when mixing different secondary organic aerosol types, *Atmos. Chem. Phys.*, 2022, **22**, 13783–13796.

62 S. J. Richardson, P. A. Staniec, G. E. Newby, J. L. Rawle, A. R. Slaughter, N. J. Terrill, J. M. Elliott and A. M. Squires, Glycerol prevents dehydration in lipid cubic phases, *Chem. Commun.*, 2015, **51**, 11386–11389.

 © 2023 The Author(s). Published by the Royal Society of Chemistry